Developing a time-domain method for simulating statistical behavior of many-emitter systems in the presence of electromagnetic field

A. R. Hashemi [*] and M. Hosseini-Farzad [†]
Department of Physics, College of Sciences, Shiraz University, Shiraz 71946-84795, Iran

(Received 2 September 2019; published 17 January 2020)

In this paper, one of the major shortcomings of the conventional numerical approaches is alleviated by introducing the probabilistic nature of molecular transitions into the framework of classical computational electrodynamics. The main aim is to develop a numerical method which is capable of capturing the statistical attributes caused by the interactions between a group of spontaneous as well as stimulated emitters and the surrounding electromagnetic field. The electromagnetic field is governed by classical Maxwell's equations, while energy is absorbed from and emitted to the (surrounding) field according to the transitions occurring for the emitters, which are governed by time-dependent probability functions. These probabilities are principally consistent with quantum mechanics. In order to validate the proposed method, it is applied to three different test cases: directionality of fluorescent emission in a corrugated single-hole gold nanodisk, spatial and temporal coherence of fluorescent emission in a hybrid photonic-plasmonic crystal, and stimulated emission of a core-shell SPASER (surface plasmon amplification by stimulated emission of radiation). The results are shown to be closely comparable to the experimental results reported in the literature.

DOI: 10.1103/PhysRevE.101.013308

I. INTRODUCTION

Since early developments in the modern optics, light-matter interaction [1] has been the central issue in numerous applications, ranging from lasers to photonic computers. In this field, a vast amount of research has been triggered by Purcell's statement [2,3] that the behavior of a photon emitter is highly sensitive to the surrounding electromagnetic (EM) field; both the decay rate [4] and the emission power [5] of the emitter can be effectively controlled by adjusting the EM field. Such adjustment can be performed using photonic crystal cavities [6–8], metallic surfaces and nanoparticles [9,10], plasmonic structures [11,12] and hybrid photonic-plasmonic structures (HPPSs) [13]. Another fact to consider is that the emitted light itself can also affect the neighboring luminescent molecules either directly, as a short-range interaction, or by exciting photonic and/or plasmonic guided modes, which leads to a long-range interaction. In this sense, one needs to deal with complicated time-varying internal and external interactions in a many-body problem [14,15]. Therefore, further investigations are demanded to develop efficient means to control the response and enhance the emission to a higher degree for applied purposes [10].

Considering the practical limitations of the delicate experimental setups, a rather low-cost numerical method can be effectively employed to provide guidelines for experiments [16,17] while it also advances our fundamental understanding of physical phenomena [18,19]. However, the presence of numerous emitters in the vicinity of a nanostructure results in special collective attributes, e.g., coherence, which requires developing an approach to numerically capture the statistical physics of the phenomena. It is necessary to ensure that the probabilistic nature of molecular transitions is taken into account, and, consequently, one can utilize a statistical approach to infer the collective attributes. In other words, any two emitters of the ensemble that are in the same environmental condition do not deterministically behave in the same way. In addition, the numerical method should be capable of handling the interaction between emitters and the external EM field as well as the emitter-photon-emitter interactions.

Emitters can be numerically simulated using two different class of methods: those developed based on a macroscopic viewpoint, i.e. using statistically averaged quantities, like effective optical parameters, e.g., permittivity, conductivity, and wave number [18,20], or population densities for molecular energy levels [21–23]. In the second class of methods, a microscopic viewpoint is adopted, i.e., in which one focuses on the behavior of a single molecule using quantum mechanical methods, like solving the atomic master equation, density function equation, or Schrödinger's equation [24–27], or modeling the molecular dipole moment of emitters in a classical manner using a damped driven harmonic oscillator differential equation [6,28–32]. The latter approach has been frequently used in the literature due to its simplicity and capability to be implemented within the framework of conventional numerical methods developed for EM wave propagation, e.g., the finite-difference time domain (FDTD) [33].

The macroscopic viewpoint is well qualified for simulating a bulk of emitting matters; as an example, Chang and Taflove [21] successfully simulated laser gain material by developing a semiclassical approach. Nevertheless, in this viewpoint, the behavior of numerous microscopic emitters, which are

[*] arezahashemi@gmail.com
[†] hosseinif@shirazu.ac.ir

subject to identical conditions, is represented by the averaged macroscopic quantities. Therefore, despite its promising performance for a bulk of active matter, this viewpoint is not a suitable choice for cases of many emitters with individually different dipole orientations and local (especially time-dependent) heterogeneity at the molecular scale. Moreover, in this class of approaches, the probabilistic nature of problems is lost as a result of the deterministic governing equations.

On the other hand, numerical methods are developed adopting microscopic viewpoint with the quantum mechanical approach [27]. In these approaches, due to a prohibitive computational cost, the governing equation, e.g., Schrödinger's equation, including the terms corresponding to the external field-emitter and emitter-emitter interactions, can be solved only for a rather small number of emitters. This shortcoming can be resolved by considering all emitters as identical to each other [14]. However, this requires the environmental conditions to be completely the same for all the emitters. Moreover, acquiring the microscopic viewpoint with a classical approach for modeling the dipoles, one cannot make any distinction between the excitation and emission frequency in cases of three-level emitters like fluorescent molecules [34,35]. More importantly, representing the dipole moment of distinct emitters using a single deterministic equation for harmonic oscillator, the statistical nature is lost.

The subject of the present work is to show how the probabilistic nature of the molecular transitions can be microscopically taken into account while the statistical attributes of a rather large set of emitters are macroscopically calculated. To this end, a semiclassical approach is proposed, in which transition probabilities are introduced in order to handle the behavior of emitters, which are considered as single molecules with particular behavior and distributed in the computational cells. To the best of our knowledge, this is the first time that such approach has been pursued. It is worth noting that since the presented method is based on generating random samples from probability distributions in a repeated manner, it can be categorized within the broad class of Monte Carlo methods. This class of methods has shown promising performance in handling the probabilistic nature of many-body problems [17,36]. Here the introduced algorithm is implemented within the framework of the FDTD method and validated against previously reported experimental results for spontaneous and stimulated emissions: directionality and coherence of spontaneous emission and stimulated emission of a SPASER (surface plasmon amplification by stimulated emission of radiation). It is worth noting that in the present work, the implemented algorithm is developed for a three-level fluorescent molecule as the emitter. However, it is straightforward to generalize the algorithm to include two- and four-level emitters as well.

II. NUMERICAL MODELING

An emitter with three energy bands, e.g., a fluorescent molecule can be modeled as a three (energy) level system, for which absorption and both radiative and nonradiative transitions occur [37,38] (Fig. 1). From the quantum mechanical viewpoint, a time-dependent probability function can be associated with each of these possible transitions. In the

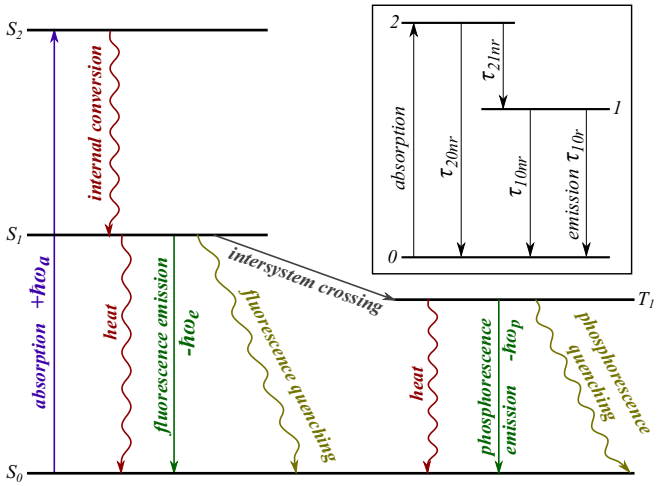

FIG. 1. Jablonski diagram showing electronic transitions of a molecule with radiative and nonradiative transitions from or to singlet (S) and triplet (T) states. The simplified model for a fluorescent molecule is shown in the inset.

following, the implementation of these probability functions within the framework of a time-domain method, which is originally developed for simulating EM field propagation, is briefly described for a many-emitter system. For more convenience in this paper, the subscripts are corresponding to the energy levels as numbered in Fig. 1. Moreover, the energy levels of each molecule are identified using three occupation numbers n_0, n_1, and n_2, where at each time step, only one of them is 1 while the other two are 0. This is due to the fact that at any instance of time, only one of the energy levels can be occupied by the molecule. Here t is the total time of the simulation, while $\tilde{t}$ is the time passed from the last transition occurred for the molecule, P_{ij} is the time-dependent probability of transition from level i to level j, and the subscripts r and nr refer to the radiative and nonradiative transitions, respectively.

At each time step, the state is checked for each molecule in the system according to the following criteria:

(1) For a molecule in the ground state ($n_0 = 1$), it is only possible to transit into the second excited state ($0 \xrightarrow{\text{absorb}} 2$) by absorbing an enough amount of energy. Computationally, this occurs if the randomly generated number $0 < r < 1$ is less than (or equal to) the corresponding probability $P_{02}(t)$.

(2) For a molecule in the second excited state ($n_2 = 1$), the nonradiative decay is possible to either the first state ($2 \xrightarrow{nr} 1$) or the ground state ($2 \xrightarrow{nr} 0$). If random number r is less than (or equal to) $P_{21nr}(\tilde{t})$ transition $2 \xrightarrow{nr} 1$ occurs, and on the other hand, the molecule experiences $2 \xrightarrow{nr} 0$ if $P_{21nr}(\tilde{t}) < r \leqslant [P_{21nr}(\tilde{t}) + P_{20nr}(\tilde{t})]$.

(3) For a molecule in the first excited state ($n_1 = 1$), both the radiative and nonradiative decays to the ground state are possible. Transition $1 \xrightarrow{nr} 0$ occurs if $r \leqslant P_{10nr}(\tilde{t})$. Otherwise, if $P_{10nr}(\tilde{t}) < r \leqslant [P_{10nr}(\tilde{t}) + P_{10r}(\tilde{t})]$, the radiative transition of $1 \xrightarrow{r} 0$ takes place, and consequently, a wave packet with the central frequency equal to emission frequency of the

fluorophore ω_e is emitted from a point source at the position of the emitting molecule.

Once a transition occurs, the occupation numbers n_0, n_1, and n_2 are correspondingly reset, e.g., $0 \overset{\text{absorb}}{\rightarrow} 2$ is associated with resetting numbers as $n_0 = 0$ and $n_2 = 1$. During emission, the re-excitation of the corresponding molecule is prevented by setting its emission flag to *on*, which means the state of the molecule is ignored and the emission continues until the emitted wave packet vanishes. At this moment, the emission flag is off and the molecule is at its ground state.

The probabilities associated with the above-mentioned transitions between these levels are estimated as described in the following. It is evident that these probabilities can be modified into more sophisticated functions that are obtained by quantum mechanical analysis of molecules. However, the following formulas show the simplest probability functions that satisfy the physical requirements and work successfully for the test cases solved in this work.

A. Absorption

For a molecule with the frequency of the maximum absorption, ω_a, the absorption of energy from the field and excitation of the molecule becomes more probable if the electric field imposed at the position of molecule, $\mathbf{E}(t)$, incorporates a frequency component tending to ω_a. In order to examine this possibility, the occurrence of the resonance of a harmonic oscillator driven by $\mathbf{E}(t)$ is checked. This oscillator resembles the electric dipole moment of the molecule, $\mathbf{p}$. Within the context of the time-domain method used in the present work, i.e., FDTD, the equation that governs the response of the harmonic oscillator is considered as an auxiliary differential equation (ADE) [39]. It must be highlighted that using the aforementioned ADE is the most efficient way to check the frequency components of $\mathbf{E}(t)$ against ω_a. The implemented ADE is

$$\ddot{p} + \gamma \dot{p} + \omega_a^2 p = (e^2/m)\mathbf{E}(t) \cdot \hat{\mathbf{p}}. \tag{1}$$

Here γ is a damping factor and e and m are the charge and mass of electron, respectively. Vector $\hat{\mathbf{p}}$ is a unit vector representing the orientation of dipole moment of the emitter, $\mathbf{p} = p\hat{\mathbf{p}}$. The magnitude of the dipole moment is initially zero and updated (at time step $n+1$) using a second-order central time-marching scheme as done for Maxwell's equations in the adopted FDTD method [33]. At the onset of resonance, the amplitude of $\mathbf{p}$ tends to its maximum value $p_{\max}$, and consequently, the transition from level 0 to 2 becomes more probable. Therefore, the corresponding probability is estimated as

$$P_{02}(t_n) = \exp\{-[p(t_n) - p_{\max}]^2/2\sigma^2\}, \tag{2}$$

where t_n represents time at nth time step, i.e., $t_n = n\Delta t$, and σ is determined in terms of the absorption bandwidth of the fluorophore, $\Delta\omega_a$. In order to derive an equation for σ, one can consider the external field in its simplest form $\mathbf{E}(t) = \mathbf{E_0}\sin(\omega t)$ and analytically solve Eq. (1) for the amplitude of

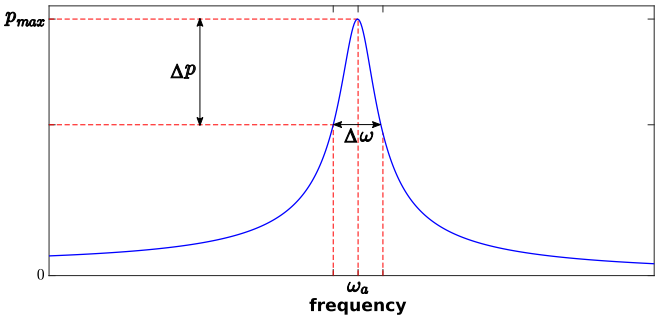

FIG. 2. Amplitude of $\mathbf{p}$ as a function of ω.

$\mathbf{p}$, which depends on ω as

$$p(\omega) = \frac{(e^2/m)|E_0|}{\sqrt{\left(\omega_a^2 - \omega^2\right)^2 + (\gamma\omega)^2}}. \tag{3}$$

As illustrated in Fig. 2, for an absorption bandwidth of $\Delta\omega_a$, an amplitude interval of Δp is defined as

$$\Delta p = p_{\max} - p\left(\omega_a - \tfrac{\Delta\omega_a}{2}\right). \tag{4}$$

In this way, the standard deviation σ is considered equal to Δp. It must be noted that since $p_{\max} \propto \frac{1}{\gamma\omega_a}$, both $p_{\max}$ and damping factor γ are arbitrary factors which should be determined correspondingly.

Upon the occurrence of resonance, energy is also absorbed from the external EM field, which is governed by Ampère-Maxwell's relation:

$$\varepsilon\dot{\mathbf{E}} = \nabla \times \mathbf{H} - \sum_{i=1}^{N} \dot{\mathbf{p}}_i.$$

Here N denotes the number of fluorophores associated with the computational grid cell, which is proportional to the density of the fluorescent material at the same point within the FDTD discretized domain. It is possible to have various fluorescent densities at different locations of the structure. If referring to Eq. (2) transition $0 \overset{\text{absorb}}{\rightarrow} 2$ occurs, p and its first temporal derivative are set to zero. On the other hand, if $0 \overset{\text{absorb}}{\rightarrow} 2$ does not occur, the dipole moment of the molecule is updated via Eq. (1).

B. Nonradiative transitions

For the present model, three nonradiative transitions are considered: $2 \overset{nr}{\rightarrow} 1$, $2 \overset{nr}{\rightarrow} 0$, and $1 \overset{nr}{\rightarrow} 0$. The corresponding probabilities are estimated as

$$P_{21nr}(\tilde{t}) = A\left[1 - \exp\left(-\frac{\tilde{t}}{\tau_{21nr}}\right)\right], \tag{5}$$

$$P_{20nr}(\tilde{t}) = B\left[1 - \exp\left(-\frac{\tilde{t}}{\tau_{20nr}}\right)\right], \tag{6}$$

$$P_{10nr}(\tilde{t}) = C\left[1 - \exp\left(-\frac{\tilde{t}}{\tau_{10nr}}\right)\right]. \tag{7}$$

Here τ_{ijnr} represents the time constant for a nonradiative decay between levels i and j. The asymptotic behavior of these functions guaranties a definite decay at an infinitely long time.

C. Radiative transition

Radiative transition is considered only as a decay from level 1 to level 0, for which the corresponding probability is estimated as

$$P_{10r}(\tilde{t}) = D\Big[1 - \exp\Big(-\tfrac{\tilde{t}}{\tau_{10r}}\Big)\Big], \tag{8}$$

where τ_{10r} is the time constant of the radiative decay. Once the transition occurs, a wave packet is emitted with a central frequency equal to the emission frequency of the fluorophore, ω_e. This is implemented as a soft point source, which is a vector function, $\mathbf{F}(\tilde{t})$, that is superimposed to the electric (and/or magnetic) field at the position of the molecule. This function is formulated as

$$\mathbf{F}(\tilde{t}) = \mathbf{F}_0 \exp\left[-\frac{(\tilde{t}-t_0)^2}{\sigma_e^2}\right] \sin[\omega_e(\tilde{t}-t_0)], \tag{9}$$

where $\mathbf{F}_0 = F_0\hat{\mathbf{n}}$. In this equation, $\hat{\mathbf{n}}$ is a randomly oriented unit vector and F_0 is determined in a manner that the total energy of the wave packet is equal to the energy of an emitted photon. Here σ_e is associated with the bandwidth of the emission and $t_0 \approx 3\sigma_e$ is a time offset, which guarantees that at $\tilde{t} = 0$, $\mathbf{F}$ approaches zero.

The normalization factors A, B, C, D are calculated based on two physical concepts; first, it is impossible for a molecule to permanently stay at an excited state, and consequently, $A + B = 1$ and $C + D = 1$. Second, the probability ratio of the transitions is inversely related to the corresponding decay times, τ_{ij}. Therefore, one can obtain

$$A = \tau_{21nr}/(\tau_{21nr} + \tau_{20nr}), \qquad B = \tau_{20nr}/(\tau_{21nr} + \tau_{20nr}),$$
$$C = \tau_{10nr}/(\tau_{10nr} + \tau_{10r}), \quad \text{and} \quad D = \tau_{10r}(\tau_{10nr} + \tau_{10r}).$$

The flowcharts illustrated in Figs. 3 and 4 present the implemented algorithm in more detail.

In this work, the propagation of EM fields in a three-dimensional domain and successive time steps is simulated using an FDTD package, which is developed in C++ language. A convolutional perfectly matched layer (CPML) [40,41] boundary condition is used for reducing the reflection from exterior boundaries of the simulation domain. Whenever needed, the total-field–scattered-field technique and the Drude-Lorentz model are implemented to handle the incident field and dispersive materials, respectively [33]. In all simulations, the electric and magnetic fields are initially set to zero. It is worth noting that the implementation of the same algorithm is also possible for other numerical methods, e.g., the finite-element time-domain method.

III. APPLICATIONS FOR MANY SPONTANEOUS EMITTERS

In the following, the proposed method is applied to two phenomena observed for many-emitter systems; directionality of fluorescence in the presence of a plasmonic nanostructure [42] and fluorescence coherence obtained utilizing an HPPS [13]. The present method is validated by comparing the numerical results with the corresponding experimental results reported in the literature.

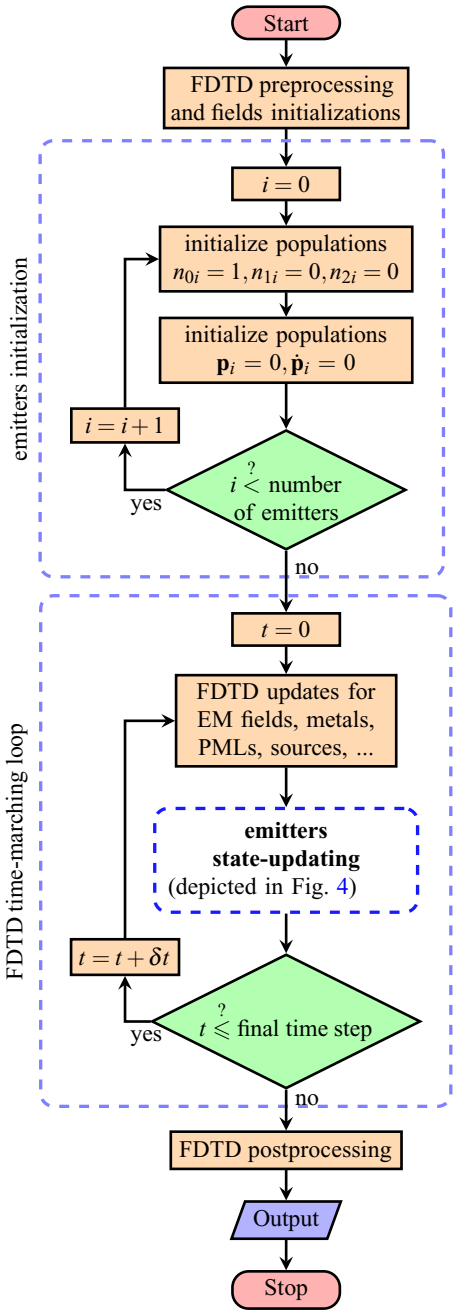

FIG. 3. The modified FDTD algorithm for implementing the procedure required for simulating emitters-EM field interactions. All emitters are at the ground state at the beginning of simulation and updated during the main time-marching loop. The state-updating steps are elaborated in Fig. 4.

Here the spatial discretization of the solution domain is set considering the criteria for minimizing the dispersion error of the FDTD method [33] while resolving all structural details. Governing equations are solved for a three-dimensional Cartesian mesh with Yee cells of $\Delta x = \Delta y = \Delta z$. The time step is set according to the Courant condition. The physical properties of the specific emitters simulated in the present work are shown in Table I.

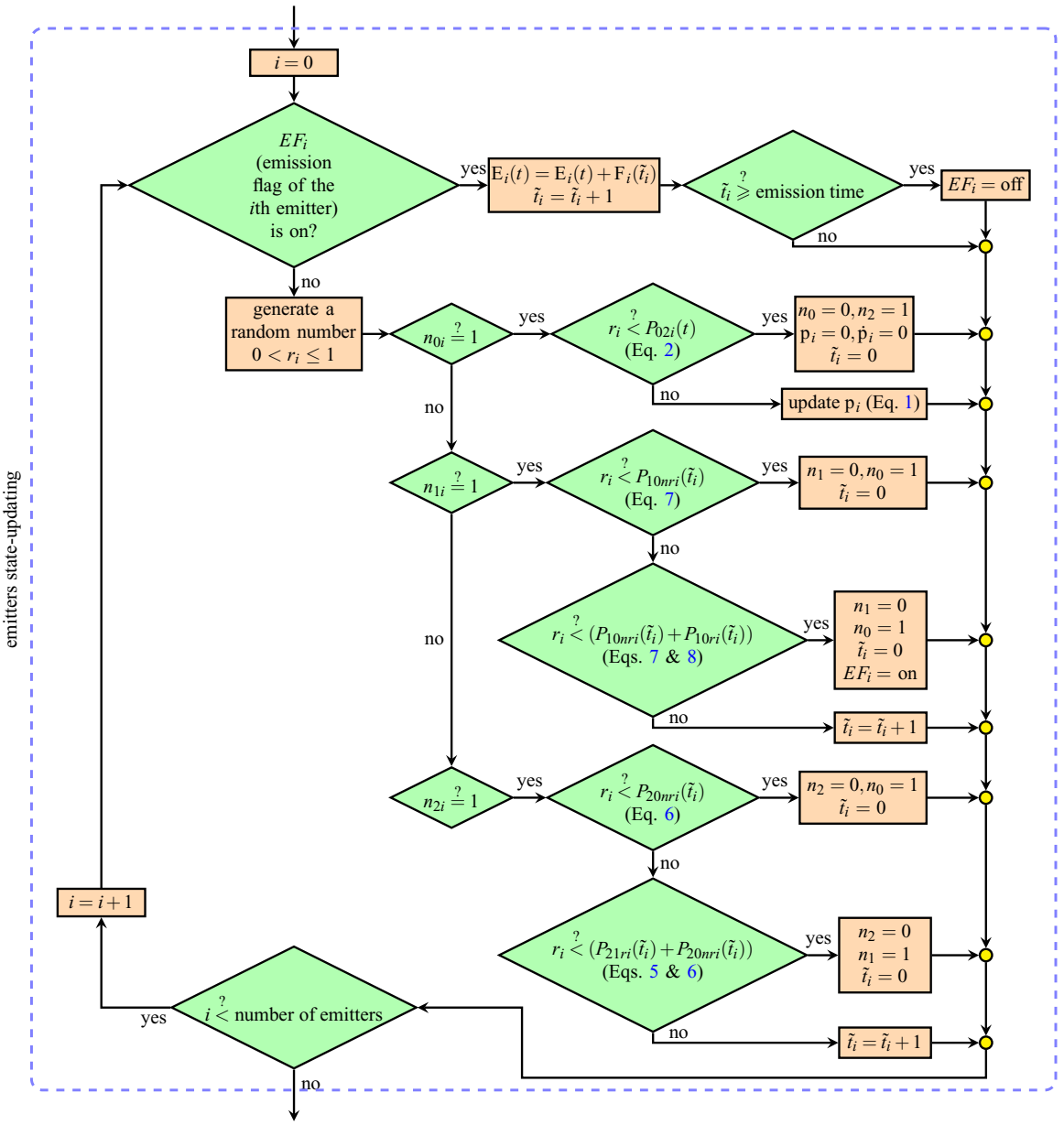

FIG. 4. State-updating procedure for emitters. In this flowchart, EF_i is the emission flag of ith emitter, which is *on* while the wave packet is emitting. $\mathbf{E}_i(t)$ is the electric field at the position of the ith emitter, $\mathbf{F}_i(\tilde{t}_i)$ is the emitted electric wave function, and t_i is the time elapsed since the ith emitter has been transited to its current state. In each time step, if the emission flag of an emitter (e.g., the ith one) is on, the emission continues. If the flag is off, the state of the emitter should be checked. In case the emitter is at the ground state, the absorption probability $P_{02i}(t)$ is compared to a randomly generated number, r_i, and consequently, either the transition to level 2 takes place or the dipole moment of the emitter is updated. In other cases (i.e., the emitter is at level 1 or 2) the same procedure is followed with the corresponding probability function.

TABLE I. Optical properties of emitters used in test cases.

	Excitation wavelength (nm)	Emission wavelength (nm)	Quantum yield	Excited state lifetime (ns)	τ_{10r} (ns)	τ_{10nr} (ns)	τ_{21nr} (ns)	τ_{20nr} (ns)
Alexa Fluor 647	650	672	0.3	1.04	3.5	1.7	0.01	11.4
Rhodamine 6G	525	550	0.95	4.08	4.3	92.7	0.01	824.1
Sulfohodamine 101	575	591	0.8	4.2	5.2	23.8	0.01	257.5
Oregon Green 488	494	524	0.9	4.3	4.8	48.8	0.01	265.

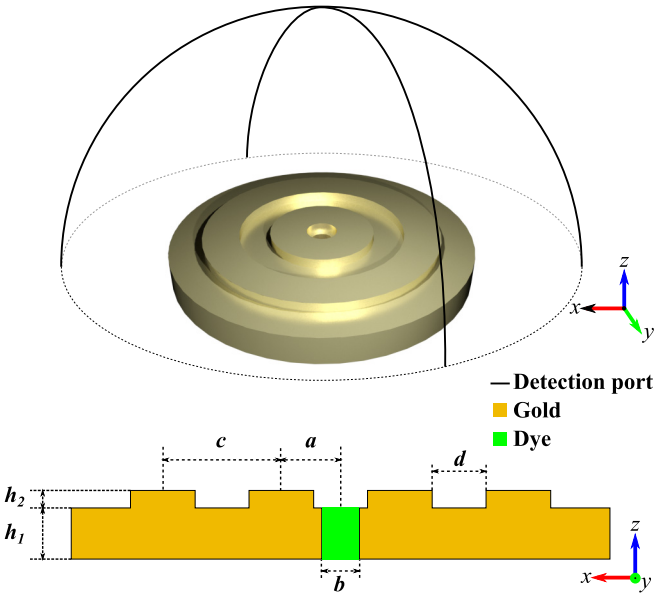

FIG. 5. Schematic of the plasmonic nanodisk with the fluorescent molecules positioned at the central hole of it as proposed by Aouani *et al.* [42]. The three-dimensional view is shown on top, and the cross-sectional view is presented at the bottom. The geometrical parameters are set according to [42] as $a = 220$ nm, $b = 140$ nm, $c = 440$ nm, $d = 200$ nm, $h_1 = 190$ nm, and $h_2 = 65$ nm.

A. Directional spontaneous emission

In this section, the central hole of a gold nanodisk with two concentric grooves is filled by excited fluorescent molecules as shown in Fig. 5. The capability of this plasmonic system in producing directional emission has been experimentally studied by Aouani *et al.* [42]. The geometrical parameters (see Fig. 5), as well as the physical properties of the base structure (gold) and the fluorescent (Alexa Fluor 647 and rhodamine 6G) molecules, are set the same as those reported in Ref. [42]. The properties of Alexa Fluor 647 and rhodamine 6G are set according to Refs. [43] and [44], respectively (see Table I). In this test case, the caution is that the resulted emission distribution is hardly distinguishable due to the masking effect of the incident pump beam. Here in order to eliminate the need for a postprocessing procedure, the fluorophore molecules are considered to be initially excited ($n_2 = 1$ for all molecules). In this way, there is no need to impose a pump beam.

Here two different simulations are separately done one for Alexa Fluor 647 and one for rhodamine 6G molecules as the fluorescent molecules, while the output emission is detected at two perpendicular arc ports on the hemisphere encircling the disk as illustrated in Fig. 5. The long-time average as well as the ensemble average of the intensity are presented in Fig. 6. The results are in a good agreement with those reported in Ref. [42] (see Fig. 6, dashed lines), i.e., for Alexa Fluor 647 the peak intensity is observed at a polar angle of around 27°, while for rhodamine 6G the emission becomes concentrated at the zero polar angle.

B. Fluorescence coherence

The main aim of developing the proposed method is to capture the statistical attributes of a many-emitter system. In this sense, the method is utilized to simulate the response of a set of fluorescent molecules positioned adjacent to a photonic crystal (PC) constructed by triangular arrangement of polystyrene spheres of 500 nm diameter. This PC is placed on top of a 200-nm-thick silver slab to form an HPPS as shown in Fig. 7. The incident pump ($\lambda = 532$ nm) works continuously in the y direction, while the output emission is detected in the z direction. The capability of this structure in producing a coherent light from fluorescent spontaneous emissions was previously reported by Shi *et al.* [13]. Coherence of a fluorescent light is one of the statistical phenomena which to the best of authors' knowledge has not yet been numerically addressed. In this case, the fluorescent material, fluorophore-doped polyvinil alcohol (PVA), forms a 50-nm-thick layer on top of the HPPS and also fills the vacancy between spheres (see the cross-sectional view in Fig. 7). In order to keep the numerical test case substantially similar to the reported experimental setup, properties of the fluorophores, i.e., excitation and emission wavelength, are set according to the physical properties of sulforhodamine 101 (S101) as $\lambda_{ex} = 575$ nm and $\lambda_{em} = 591$ nm, respectively (Table I). A y-directed 532 nm continuous wave is used to pump the structure from the center of the x-z plane.

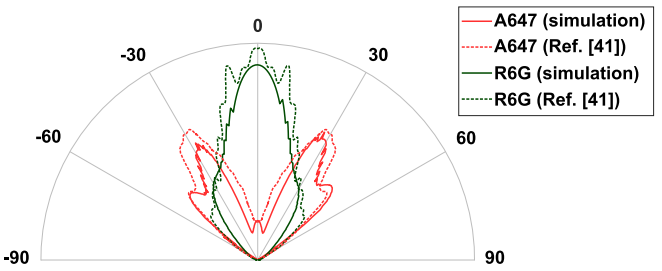

FIG. 6. Polar distribution of the long-time and ensemble averaged intensity for emissions detected from the plasmonic nanodisk. Red (light gray) and green (dark gray) curves correspond to the results obtained for Alexa Fluor 647 ($\lambda_{em} = 670$ nm) and rhodamine 6G ($\lambda_{em} = 560$ nm), respectively. Numerical results (solid lines) are compared with the results reported by Aouani *et al.* [42] (dashed lines).

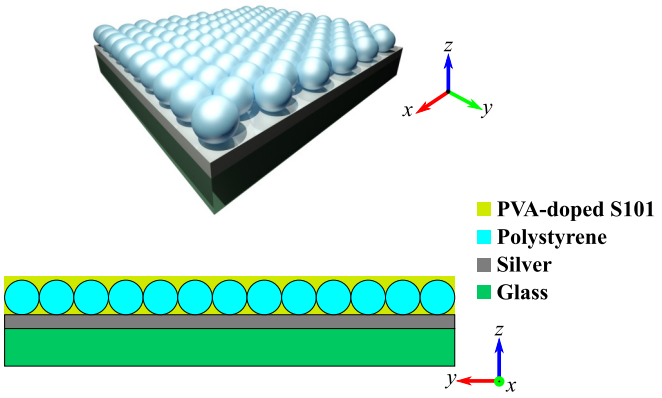

FIG. 7. Schematic of the HPPS proposed by Shi *et al.* [13]. The y-z cross-sectional view of the structure is shown at the bottom, in which the fluorescent-doped PVA filling is also marked.

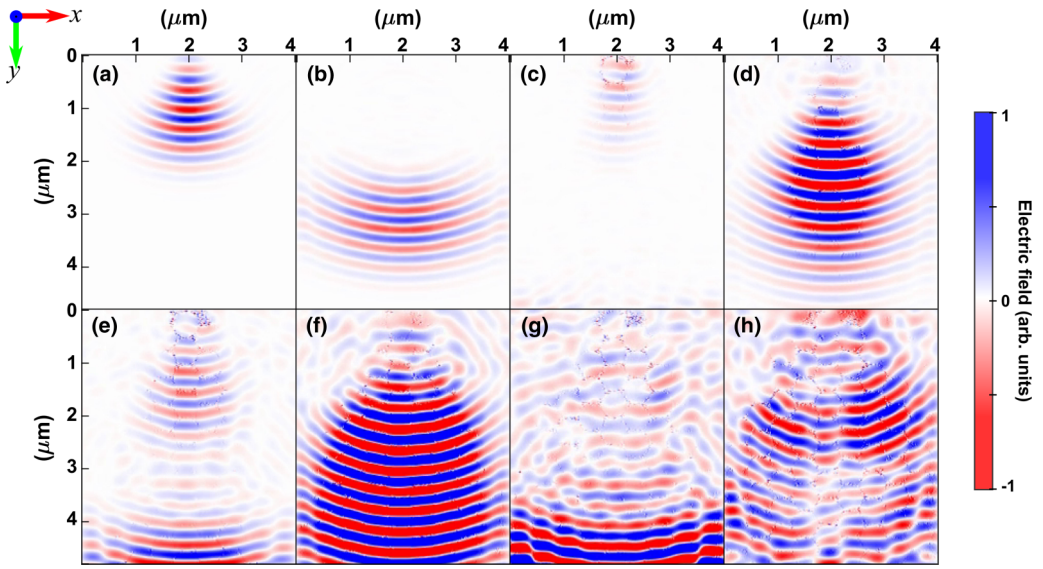

FIG. 8. The time evolution of the electric field produced by a pulse train in the photonic-crystal part of the HPPS proposed by Shi *et al.* [13]. The field distribution on a surface passing through the center of the polystyrene spheres in the *x*-*y* plane (see the structure in Fig. 7) is illustrated at selective time steps. The *y*-directed incident pump pulse enters the domain of the structure from the center of *x*-*z* plane ($y = 0$). Here the first four pulses of the train are depicted. The fluorescent emission of the molecules is observed as small spots disturbing the pump field.

In Fig. 8 the time evolution of the field distribution is plotted on a surface passing through the center of the polystyrene spheres in the *x*-*y* plane. Since the low-intensity fluorescent emissions are masked by the pump intensity, which would result in an unclear field distribution, here the results are plotted merely for a pulse train. It is worth noting that for all other simulations of the current test case, the continuous wave is used. It is observed that the first pump pulse passes through the domain without any fluorescent molecule emission [Fig. 8(b)]. The fluorescent emission is seen in Figs. 8(c)–8(h) since the molecules have gained the excitation energy required for emission. The honeycomb-like pattern [seen more clearly in Fig. 8(g) and 8(h)] is caused by the fluorescent emission of molecules filling the vacancy between the polystyrene spheres.

In order to estimate the degree of temporal coherence, two different approaches have been employed: in one approach, the temporal coherence function (TCF) is utilized, which is the autocorrelation of the signal,

$$\Gamma(\tau) = \langle u(t+\tau)u^*(t)\rangle,$$

where angle brackets and the asterisk superscript denote the time averaging and complex conjugate, respectively [45]. Here $u(t)$ is the electric field. The degree of coherence is conclusively determined as $\gamma(\tau) = \Gamma(\tau)/\Gamma(0)$, and, thus, the coherence time is

$$\tau_c = \int_{-\infty}^{\infty} |\gamma(\tau)|^2 \, d\tau. \tag{10}$$

Using this approach for the present test case, the coherence time is $\tau_c = 1.14 \times 10^{-13}$ sec; this is approximately equivalent to the wavelength bandwidth of $|\Delta\lambda| = 6.9$ nm. In the other approach, the desirable wavelength spectrum is obtained using the Fourier transform of the time-varying electric field. For the present test case, this spectrum is shown in Fig. 9. By fitting a Gaussian function into the figure, the emission bandwidth of the peak is calculated to be approximately $|\Delta\lambda| = 7.1$ nm.

It must be noted that in the present work, a perfectly ordered structure is modeled, while any experimental test is subject to fabrication defects. These structural defects lead to a wider bandwidth, and, therefore, a lower temporal coherence can be detected for the experimental setup. This is due to the fact that any defect or disorder perturbs the Hamiltonian of the structure, which in turn broadens the band of energy [46]. Considering this issue, there is a good agreement between the result obtained using the proposed numerical method and the $|\Delta\lambda| = 9$ nm bandwidth reported in the literature [13].

On the other hand, the most reliable and extremely practical approach to the estimation of spatial coherence is the Young's double-slit technique [47] for which the interference

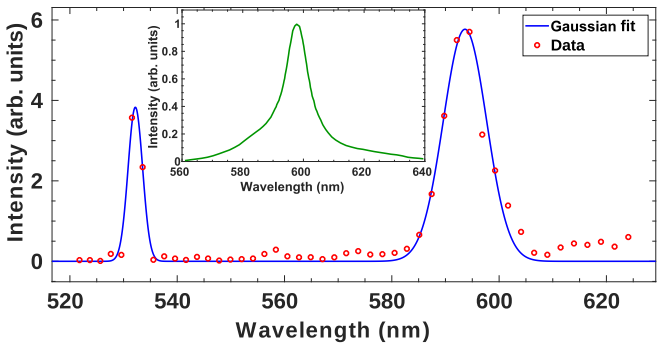

FIG. 9. Wavelength spectrum that is obtained using the proposed numerical method. The peak corresponding to the reflected portion of the excitation wave is observed at $\lambda = 532$ nm, and the emission peak occurs at $\lambda = 594$ nm with the bandwidth of $|\Delta\lambda| = 7.1$ nm. The inset shows the emission spectrum as reported by Shi *et al.* [13].

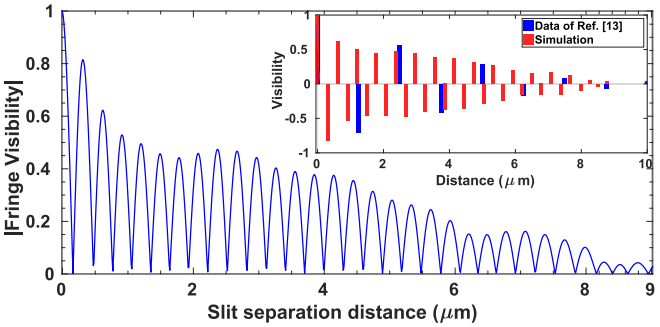

FIG. 10. Young's double-slit fringe visibility as a function of the separation distance of the double slits calculated using the proposed numerical method. The main plot shows the absolute value of visibility, and in the inset, the maxima and minima of visibility are plotted as red (light gray) bars. The results reported in Fig. 4(c) of Ref. [13] are also plotted as blue (dark gray) bars for comparison.

fringe visibility is analytically calculated as a function of the separation distance between slits as [45]

$$\mathcal{V}_{ij} = \frac{2\sqrt{u_i^2(t)u_j^2(t)}}{u_i^2(t)+u_j^2(t)} M_{ij}.$$

In this equation,

$$M_{ij} = \frac{\langle u_i(t)u_j^*(t)\rangle}{\sqrt{\langle u_i^2(t)\rangle\langle u_j^2(t)\rangle}}$$

is the mutual coherence function between electric fields $u_i(t)$ and $u_j(t)$ detected at two distinct points i and j placed on a plane perpendicular to the direction of detection, which represent the positions of the slits. For the present test case, the fringe visibility is plotted in Fig. 10. It is evident that visibility significantly decreases as the slits' separation distance increases beyond 4 μm, and practically, no interference pattern can be observed for a separation distance of larger than 8 μm. This is in close agreement with the result reported in Ref. [13]; clearly visible interference fringes were observed for the slit-separation distance of 4 μm, and less clear interference fringes were recognized for the slit-separation distance of 7 μm. Nevertheless, it is noteworthy that using numerical simulation, it can be observed (Fig. 10) how the fringe visibility varies for a wide range of separation distances. In Fig. 10 (inset), the maxima and minima of the visibility calculated using the proposed numerical method are plotted. In this figure, the intensity of modes as a function of propagation length as reported by Shi *et al.* [13] is also illustrated for comparison.

IV. EXTENDING THE PROPOSED METHOD

One of the main advantages of the proposed method is its capability to be modified for other applications beyond many spontaneous emitters by modifying the probability functions. In this section, the proposed method is modified to capture the statistical behavior of a many-emitter system, which also exhibits stimulated transitions besides the spontaneous transitions. To this end, it is needed to modify the proposed algorithm in order to also include the probability function $P_{10\text{stim}}$ required to model the stimulated emission transition. This probability should be based on transition-field coupling and thus can be defined analogously to Eq. (2) as

$$P_{10\text{stim}}(t_n) = \exp\left[-(p_{\text{stim}}(t_n) - p_{\text{stim,max}})^2/2\sigma_{\text{stim}}^2\right], \quad (11)$$

where p_{stim} is obtained using the following harmonic oscillator equation:

$$\ddot{p}_{\text{stim}} + \gamma_{\text{stim}}\dot{p}_{\text{stim}} + \omega_e^2 p_{\text{stim}} = (e^2/m)|\mathbf{E}(t)|. \quad (12)$$

Here the subscript *stim* corresponds to the stimulated transition, and ω_e is the frequency of the stimulating photons. It must be noted that upon transition a wave packet of the form

$$\mathbf{F}_{\text{stim}}(\tilde{t}) = \mathbf{F}_{\text{stim},0}\exp\left[-\frac{(\tilde{t}-t_{\text{stim},0})^2}{\sigma_{\text{stim,e}}^2}\right] \times \sin[\omega_e(\tilde{t}-t_{\text{stim},0})] \quad (13)$$

is emitted. Since the polarization of a photon released in stimulated emission must be aligned with the polarization of the stimulating photon, the amplitude of the wave packet is $\mathbf{F}_{\text{stim},0} = F_0\hat{\mathbf{E}}(t)$, where $\hat{\mathbf{E}}(t)$ represents the unit vector aligned with the electric field at the position of the molecule and the instance of stimulated transition. It is worth noting that the previously proposed semiclassical FDTD approaches (for example, see Refs. [21] and [23]) incorporate the statistically averaged quantities from a deterministic viewpoint. Therefore, those methods are capable only of modeling a bulk of emitting material, in contrast to many-emitter systems with localized sources that are successfully simulated using the present method.

In order to verify the performance of the proposed method, a core-shell-type surface plasmon amplification by stimulated emission of radiation (SPASER) is simulated, and the numerical results are compared to the experimental results reported by Noginov *et al.* [48]. The structure is schematically shown in Fig. 11; the core is made of gold with a diameter of 14 nm, which is enclosed by an Oregon Green 488 (see Table I) doped silica shell of 44 nm diameter. Here the goal is only to investigate the performance of the method in simulating stimulated emission, and, hence, the pump mechanism is considered to be out of scope. In this sense, an initial energy-level population inversion is considered for the dye molecules; i.e., all Oregon Green 488 molecules are initially at level 2. The emission spectrum is shown in Fig. 12, which shows two peaks around $\lambda_{\text{spon}} = 520$ nm corresponding to the spontaneous emission and $\lambda_{\text{stim}} = 540$ nm corresponding to the stimulated emission. Here the peak wavelengths are calculated by matching two Lorentzian functions to the data as illustrated in Fig. 12. The agreement between these results and those reported in Ref. [48], i.e., $\lambda_{\text{spon}} = 520 \pm 20$ nm and $\lambda_{\text{stim}} = 531$ nm, approves the validity of the proposed method for many-spontaneous and stimulated emitters (see the inset of Fig. 12). However, the slight deviation in λ_{stim} caused by the so-called staircase error generally occurs in the FDTD method. In the experimental case, the stimulated emission results from the feedback provided by the surface plasmons of the core inside a cavity of a spherical shape. In the FDTD

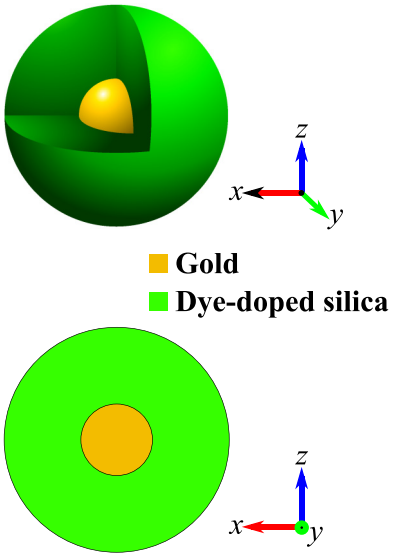

FIG. 11. Schematic of the core-shell-type SPASER.

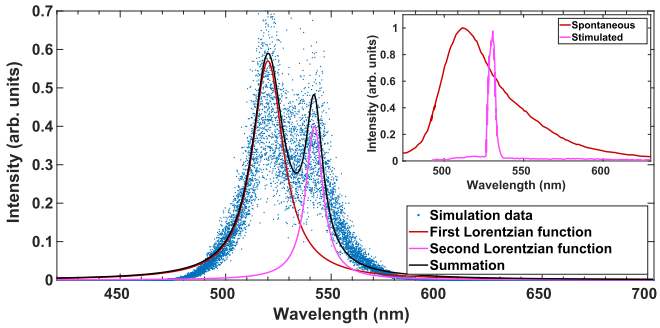

FIG. 12. Emission spectrum of SPASER. The Lorentzian functions and their summation are matched to the data and shown in red (dark gray), purple (light gray), and black, respectively. The results reported by Noginov *et al.* [48] are shown in the inset.

simulation, on the other hand, the spheres cannot exactly be fitted by the Cartesian grid. Here mapping of the faces onto the computational cells leads to the appearance of some stairs at the surface of the spheres. Thus, the resonance modes of the numerically modeled simulated sphere are slightly different from those of a real spherical cavity, and consequently, the peak of the stimulated emission obtained in the simulation is slightly different than that of the experiment. In order to alleviate this error one needs to either use a highly refined domain discretization that needs prohibitively intense computations or utilize a body-fitted grid, which is out of the scope of the present work.

V. CONCLUSION

A numerical method was developed which is capable of capturing the statistical nature of the interactions between a group of emitters and the surrounding EM field. The proposed algorithm was devised in a manner that is basically consistent with physical principles. The method has been validated for three different many-emitter systems. In the first test case, the directionality of the fluorescent emission is captured. In the second test case, the spatial and temporal coherence are simulated for an ensemble of spontaneous emitters. This important statistical attribute can be numerically captured merely by utilizing the proposed probabilistic approach. In order to show the capability of the proposed method beyond the spontaneous emitters, in the last test case, the stimulated emission of a SPASER is simulated.

It is evident that the applications of the proposed method are not limited to the test cases simulated in this work; the method can be utilized to capture other statistical attributes, e.g., transition rates. In addition, by using different probability functions and/or including two or four energy levels, the method can be further developed for numerous cases with various types of emitters. Acquiring intensity-dependent probability functions is also a means to obtain more realistic physics. Moreover, nonlinear effects, e.g., two-photon absorption or up-conversion, are possible to be captured by adding virtual states and considering corresponding transitions in the algorithm.

It is worth noting that, using the proposed method, the run times are increased by less than 5% compared to a sole electromagnetic solver; however, the computational costs (memory and run-time) depend on the number of emitters. Considering the complexities and costs associated with experiments, the proposed method is a promising means to facilitate new designs for optical structures and advance the fundamental understanding of the statistical phenomena in the field of light-matter interaction.

[1] A. Frisk Kockum, A. Miranowicz, S. De Liberato, S. Savasta, and F. Nori, Ultrastrong coupling between light and matter, Nat. Rev. Phys. **1**, 19 (2019).

[2] E. M. Purcell, Spontaneous emission probabilities at radio frequencies, in *Confined Electrons and Photons: New Physics and Applications*, edited by E. Burstein and C. Weisbuch (Springer US, Boston, 1995), pp. 839–839.

[3] M. Pelton, Modified spontaneous emission in nanophotonic structures, Nat. Photonics **9**, 427 (2015).

[4] C. D. Geddes and J. R. Lakowicz, *Radiative Decay Engineering*, Topics in Fluorescence Spectroscopy Vol. 8 (Springer, Boston, 2005).

[5] K. J. Russell, T.-L. Liu, S. Cui, and E. L. Hu, Large spontaneous emission enhancement in plasmonic nanocavities, Nat. Photonics **6**, 459 (2012).

[6] D. Englund, D. Fattal, E. Waks, G. Solomon, B. Zhang, T. Nakaoka, Y. Arakawa, Y. Yamamoto, and J. Vučković, Controlling the Spontaneous Emission Rate of Single Quantum Dots in a Two-Dimensional Photonic Crystal, Phys. Rev. Lett. **95**, 013904 (2005).

[7] A. F. Koenderink, M. Kafesaki, C. M. Soukoulis, and V. Sandoghdar, Spontaneous emission in the near field of two-dimensional photonic crystals, Opt. Lett. **30**, 3210 (2005).

[8] J. L. Zhang, S. Sun, M. J. Burek, C. Dory, Y.-K. Tzeng, K. A. Fischer, Y. Kelaita, K. G. Lagoudakis, M. Radulaski, Z.-X. Shen, N. A. Melosh, S. Chu, M. Lončar, and J. Vučković, Strongly cavity-enhanced spontaneous emission from silicon-vacancy centers in diamond, Nano Lett. **18**, 1360 (2018).

[9] K. T. Shimizu, W. K. Woo, B. R. Fisher, H. J. Eisler, and M. G. Bawendi, Surface-Enhanced Emission from Single Semiconductor Nanocrystals, Phys. Rev. Lett. **89**, 117401 (2002).

[10] T. Ribeiro, C. Baleizão, and J. P. S. Farinha, Artefact-free evaluation of metal enhanced fluorescence in silica coated gold nanoparticles, Sci. Rep. **7**, 2440 (2017).

[11] A. Kinkhabwala, Z. Yu, S. Fan, Y. Avlasevich, K. Müllen, and W. E. Moerner, Large single-molecule fluorescence enhancements produced by a bowtie nanoantenna, Nat. Photonics **3**, 654 (2009).

[12] L. Shi, T. K. Hakala, H. T. Rekola, J.-P. Martikainen, R. J. Moerland, and P. Törmä, Spatial Coherence Properties of Organic Molecules Coupled to Plasmonic Surface Lattice Resonances in the Weak and Strong Coupling Regimes, Phys. Rev. Lett. **112**, 153002 (2014).

[13] L. Shi, X. Yuan, Y. Zhang, T. Hakala, S. Yin, D. Han, X. Zhu, B. Zhang, X. Liu, P. Törmä, W. Lu, and J. Zi, Coherent fluorescence emission by using hybrid photonic–plasmonic crystals, Laser Photonics Rev. **8**, 717 (2014).

[14] M. Richter, M. Gegg, T. S. Theuerholz, and A. Knorr, Numerically exact solution of the many emitter–cavity laser problem: Application to the fully quantized spaser emission, Phys. Rev. B **91**, 035306 (2015).

[15] G. S. Agarwal, Master-equation approach to spontaneous emission. III. Many-body aspects of emission from two-level atoms and the effect of inhomogeneous broadening, Phys. Rev. A **4**, 1791 (1971).

[16] M. Bradford and J.-T. Shen, Numerical approach to statistical properties of resonance fluorescence, Opt. Lett. **39**, 5558 (2014).

[17] S. Y. Lee and M.-A. Mycek, Hybrid Monte Carlo simulation with ray tracing for fluorescence measurements in turbid media, Opt. Lett. **43**, 3846 (2018).

[18] H. Cao, J. Y. Xu, S.-H. Chang, and S. T. Ho, Transition from amplified spontaneous emission to laser action in strongly scattering media, Phys. Rev. E **61**, 1985 (2000).

[19] P. Kivisaari, M. Partanen, and J. Oksanen, Optical admittance method for light-matter interaction in lossy planar resonators, Phys. Rev. E **98**, 063304 (2018).

[20] S. C. Hagness, R. M. Joseph, and A. Taflove, Subpicosecond electrodynamics of distributed bragg reflector microlasers: Results from finite difference time domain simulations, Radio Sci. **31**, 931 (1996).

[21] S.-H. Chang and A. Taflove, Finite-difference time-domain model of lasing action in a four-level two-electron atomic system, Opt. Express **12**, 3827 (2004).

[22] A. S. Nagra and R. A. York, FDTD analysis of wave propagation in nonlinear absorbing and gain media, IEEE Trans. Antennas Propag. **46**, 334 (1998).

[23] R. W. Ziolkowski, J. M. Arnold, and D. M. Gogny, Ultrafast pulse interactions with two-level atoms, Phys. Rev. A **52**, 3082 (1995).

[24] D. Dzsotjan, A. S. Sørensen, and M. Fleischhauer, Quantum emitters coupled to surface plasmons of a nanowire: A Green's function approach, Phys. Rev. B **82**, 075427 (2010).

[25] R. Dum, P. Zoller, and H. Ritsch, Monte Carlo simulation of the atomic master equation for spontaneous emission, Phys. Rev. A **45**, 4879 (1992).

[26] S.-K. Hong, S. W. Nam, and H. J. Yang, Cooperative spontaneous emission of nano-emitters with inter-emitter coupling in a leaky microcavity, J. Opt. **17**, 105401 (2015).

[27] H. Chen, J. M. McMahon, M. A. Ratner, and G. C. Schatz, Classical electrodynamics coupled to quantum mechanics for calculation of molecular optical properties: A RT-TDDFT/FDTD approach, J. Phys. Chem. C **114**, 14384 (2010).

[28] P. Genevet, J.-P. Tetienne, E. Gatzogiannis, R. Blanchard, M. A. Kats, M. O. Scully, and F. Capasso, Large enhancement of nonlinear optical phenomena by plasmonic nanocavity gratings, Nano Lett. **10**, 4880 (2010).

[29] D. Wang, T. Yang, and K. B. Crozier, Optical antennas integrated with concentric ring gratings: Electric field enhancement and directional radiation, Opt. Express **19**, 2148 (2011).

[30] M. Bauch and J. Dostalek, Collective localized surface plasmons for high performance fluorescence biosensing, Opt. Express **21**, 20470 (2013).

[31] T. B. Hoang, G. M. Akselrod, C. Argyropoulos, J. Huang, D. R. Smith, and M. H. Mikkelsen, Ultrafast spontaneous emission source using plasmonic nanoantennas, Nat. Commun. **6**, 7788 (2015).

[32] A. Javadi, S. Mahmoodian, I. Söllner, and P. Lodahl, Numerical modeling of the coupling efficiency of single quantum emitters in photonic-crystal waveguides, J. Opt. Soc. Am. B **35**, 514 (2018).

[33] A. Taflove and S. C. Hagness, *Computational Electrodynamics: The Finite-Difference Time-Domain Method* (Artech House, Boston, 2005).

[34] D. Witthaut and A. S. Sørensen, Photon scattering by a three-level emitter in a one-dimensional waveguide, New J. Phys. **12**, 043052 (2010).

[35] D. Roy, Two-Photon Scattering by a Driven Three-Level Emitter in a One-Dimensional Waveguide and Electromagnetically Induced Transparency, Phys. Rev. Lett. **106**, 053601 (2011).

[36] K. Vishwanath, B. Pogue, and M.-A. Mycek, Quantitative fluorescence lifetime spectroscopy in turbid media: Comparison of theoretical, experimental and computational methods, Phys. Med. Biol. **47**, 3387 (2002).

[37] A. Jablonski, Efficiency of anti-Stokes fluorescence in dyes, Nature (London) **131**, 839 (1933).

[38] J. R. Albani, *Principles and Applications of Fluorescence Spectroscopy* (John Wiley & Sons, 2008).

[39] T. Kashiwa and I. Fukai, A treatment by the FD-TD method of the dispersive characteristics associated with electronic polarization, Microw. Opt. Tech. Lett. **3**, 203 (1990).

[40] J. A. Roden and S. D. Gedney, Convolution PML (CPML): An efficient FDTD implementation of the CFS-PML for arbitrary media, Microw. Opt. Tech. Lett. **27**, 334 (2000).

[41] J. Berenger, Application of the CFS PML to the absorption of evanescent waves in waveguides, IEEE Microw. Wireless Components Lett. **12**, 218 (2002).

[42] H. Aouani, O. Mahboub, E. Devaux, H. Rigneault, T. W. Ebbesen, and J. Wenger, Plasmonic antennas for directional sorting of fluorescence emission, Nano Lett. **11**, 2400 (2011).

[43] V. Buschmann, K. D. Weston, and M. Sauer, Spectroscopic study and evaluation of red-absorbing fluorescent dyes, Bioconjugate Chem. **14**, 195 (2003).

[44] D. Magde, R. Wong, and P. G. Seybold, Fluorescence quantum yields and their relation to lifetimes of rhodamine 6G and fluorescein in nine solvents: Improved absolute standards for quantum yields, Photochem. Photobiol. **75**, 327 (2002).

[45] J. W. Goodman, *Statistical Optics* (John Wiley & Sons, 2015).

[46] I. Mukherjee and R. Gordon, Analysis of hybrid plasmonic-photonic crystal structures using perturbation theory, Opt. Express **20**, 16992 (2012).

[47] W. Martienssen and E. Spiller, Coherence and fluctuations in light beams, Am. J. Phys. **32**, 919 (1964).

[48] M. A. Noginov, G. Zhu, A. M. Belgrave, R. Bakker, V. M. Shalaev, E. E. Narimanov, S. Stout, E. Herz, T. Suteewong, and U. Wiesner, Demonstration of a spaser-based nanolaser, Nature (London) **460**, 1110 (2009).